Implications of ambiguity in Antarctic ice sheet dynamics for future coastal erosion estimates

a probabilistic assessment

Verschuur, Jasper; Le Bars, Dewi; Katsman, Caroline A.; de Vries, Sierd; Ranasinghe, Roshanka; Drijfhout, Sybren S.; Aarninkhof, Stefan G.J.

DOI
10.1007/s10584-020-02769-4

Publication date
2020

Document Version
Accepted author manuscript

Published in
Climatic Change

Citation (APA)
Verschuur, J., Le Bars, D., Katsman, C. A., de Vries, S., Ranasinghe, R., Drijfhout, S. S., & Aarninkhof, S. G. J. (2020). Implications of ambiguity in Antarctic ice sheet dynamics for future coastal erosion estimates: a probabilistic assessment. *Climatic Change*, *162*(2), 859-876. https://doi.org/10.1007/s10584-020-02769-4

Climatic Change manuscript No.
(will be inserted by the editor)

Implications of ambiguity in Antarctic ice sheet dynamics for future coastal erosion estimates: a probabilistic assessment

Jasper Verschuur · Dewi Le Bars · Caroline A. Katsman · Sierd de Vries · Roshanka Ranasinghe · Sybren S. Drijfhout · Stefan G.J. Aarninkhof

Received: date / Accepted: date

Abstract Sea-level rise (SLR) can amplify the episodic erosion from storms and drive chronic erosion on sandy shorelines, threatening many coastal communities. One of the major uncertainties in SLR projections is the potential rapid disintegration of large fractions of the Antarctic ice sheet (AIS). Quantifying this uncertainty is essential to support sound risk management of coastal areas, although it is neglected in many erosion impact assessments. Here, we use the island of Sint Maarten as a case study to evaluate the impact of AIS uncertainty for future coastal recession. We estimate SLR-induced coastal recession using a probabilistic framework and compare and contrast three cases of AIS dynamics within the range of plausible futures. Results indicate that projections of coastal recession are sensitive to local morphological factors and assumptions made on how AIS dynamics are incorporated into SLR projections and that underestimating the potential rapid mass loss from the AIS can lead to ill-informed coastal adaptation decisions.

Keywords Coastal erosion · Sea-level rise · Probabilistics · Antarctica · Rapid disintegration

J. Verschuur · C.A. Katsman · S. de Vries · S.G.J. Aarninkhof
Department of Hydraulic Engineering, Delft University of Technology, Stevinweg 1, 2628 CN Delft, The Netherlands
E-mail: jasperverschuur@gmail.com

J.Verschuur · D. Le Bars and S.S. Drijfhout
Royal Netherlands Meteorological Institute, Utrechtseweg 297, 3731 GA De Bilt, The Netherlands

S.S. Drijfhout
Institute for Marine and Atmospheric Research Utrecht, Department of Physics, Utrecht University, Princetonplein 5, 3584 CC Utrecht, The Netherlands

R. Ranasinghe
Department of Water Engineering, UNESCO-IHE, 3015 DA Delft, The Netherlands

R. Ranasinghe
Water Engineering and Management, University of Twente, 7500 AE Enschede, The Netherlands

R. Ranasinghe
Harbour, Coastal and Offshore Engineering, Deltares, 2600 MH Delft, The Netherlands

1 Introduction

Coastal zones accommodate millions of people worldwide and provide immense economic, environmental and aesthetic value to society (McGranahan et al., 2007; Hallegatte et al., 2013). At least 20% of the world's sandy beaches are in a state of erosion (Luijendijk et al., 2018), and sea-level rise (SLR) will inevitably exacerbate the retreat of shorelines (Stive, 2004; FitzGerald et al., 2008; Ranasinghe and Stive, 2009; Hinkel et al., 2013; Anderson et al., 2015). Coastal managers are responsible for safeguarding the resilience of coastal communities to coastline erosion. The design and cost-efficiency of coastal defences (e.g. nourishments, setback lines) hinge critically on the likelihood and magnitude of future SLR estimates along the coast. Projections of future SLR, however, have large inherent uncertainties, in particular associated with the potential rapid disintegration of the Antarctic Ice Sheet (AIS) from runaway feedbacks such as Marine Ice Sheet Instability (MISI) (Joughin et al., 2014; Ritz et al., 2015) and Marine Ice Cliff Instability (MICI) (Pollard et al., 2015; DeConto and Pollard, 2016; Oppenheimer and Alley, 2016).

Sandy shorelines are dynamic systems (Stive et al., 2002; Ranasinghe, 2016). During storms, elevated water levels, together with extreme waves, initiate episodic retreat of the shoreline, which subsequently recovers under fairweather conditions. Traditionally, to obtain predictions of storm driven beach erosion, a numerical model is forced with a design wave and surge condition to determine the resulting design storm erosion (Carley and Cox, 2003; Callaghan et al., 2009). Storm parameters (storm surge, wave height, wave period, wave angle, storm duration) are however stochastic in nature and covary with each other, making the aforementioned traditional approach sub optimal (Callaghan et al., 2008, 2009; Corbella and Stretch, 2012). SLR is expected to increase the frequency of extreme water levels (Tebaldi et al., 2012; Buchanan et al., 2017) and will therefore contribute to an amplification of storm-induced erosion (McInnes et al., 2016; Ranasinghe, 2016).

On longer time-scales (decades/century), SLR will result in coastline recession. The 'Bruun Rule' is a commonly applied predictor of this process and estimates the re-orientation of the active cross-shore profile landward and upward to maintain its equilibrium shape, thereby moving sand from onshore to offshore (Bruun, 1954). The 'Bruun Rule' is widely criticised with respect to its accuracy but is still routinely applied by practioners worldwide, mainly due to its ease of use (Cooper and Pilkey, 2004; Stive, 2004; Ranasinghe and Stive, 2009). Ranasinghe et al. (2012) introduced an alternative approach to model SLR-induced recession. This method deviates from the 'Bruun Rule' by coupling the morphodynamics of storm erosion and longer term recession using fundamental physical concepts. In addition, it has the advantage of providing probabilistic estimates of coastline recession. This methodology has now been applied in Australia (Ranasinghe et al., 2012), The Netherlands (Li et al., 2014b), Spain (Toimil et al., 2017), Sri Lanka (Dastgheib et al., 2018, in review) and France (Le Cozannet et al., 2019), and further extended to quantify coastal erosion risk (Jongejan et al., 2016; Dastgheib et al., 2018, in review).

Given the billions of dollars of coastal assets exposed, effectively managing the coastal zone is essentially a risk-management issue (Cowell et al., 2006; Oppenheimer and Alley, 2016; Ranasinghe, 2016). Probabilistic projections of storm ero-

sion and long-term recession are therefore a necessity to guide coastal managers in making risk-informed coastal zone management decisions. Management strategies should account for the uncertainty in SLR projections including potential rapid ice sheet dynamics. However, projections of AIS are ambiguous, indicating that it is currently hard to agree on a single future probability distribution function (Kopp et al., 2017). To address this, high-end projections including recent understanding of the potential rapid mass loss from of the AIS (Le Bars et al., 2017; Kopp et al., 2017) are compared to SLR projections provided by the Intergovernmental Panel on Climate Change (IPCC). Evaluating different distribution functions provides valuable insight into tail risks (i.e. events with low-probability but large consequences), which are important for risk-averse coastal managers (Hinkel et al., 2015). However, to date, the evaluation of SLR-induced erosion tail risk within a probabilistic framework is lacking in the literature and is hence the main focus of this study.

Here, we evaluate how including different projections of AIS dynamics in SLR projections might affect the design values of coastal recession (by 2100). We consider three plausible future estimates (Section 2.2): one consistent with the AR5 report of the IPCC (AR5) (Church et al., 2013), a skewed distribution function of AIS dynamics based on Levermann et al. (2014), and a high-end scenario based on DeConto and Pollard (2016). Following the Probabilistic Coastline Recession (PCR) model introduced by Ranasinghe et al. (2012), here we use a probabilistic framework using synthetic storm sampling (SSS) (Section 2.3), and an analytical erosion and shoreline prediction model (Section 2.4) to derive estimates of future storm erosion and recession (Section 3.2). We advance prior PCR model applications by introducing SLR uncertainty into the methodology (Section 4.1).

2 Methods

2.1 Study area

The island of Sint Maarten is used as a case study to demonstrate the method. It has a rocky coastline with numerous embayed and pocket beaches. The tide is primarily diurnal with a tidal range rarely exceeding 20 cm (micro-tidal) (Kjerfve, 1981). The wave climate exhibits a seasonality with mean significant wave height between 1.5 and 2.0 m. Storms are triggered by locally generated waves, hurricane events during the North Atlantic hurricane season, and swell waves generated by intense mid-latitude storms during boreal winter (Jury, 2018).

Two beaches on the island are considered; Dawn Beach (DB) and Orient Bay (OB), which are embayed beaches that face the open ocean in the east (see Supplement Figure 1). The beaches are both reflective, without a complex dune structure or offshore bars and have typical grain size diameters (D_{50}) of 0.22 - 0.85 mm (Boon and Green, 1988).

2.2 Regional sea-level rise projections

The starting point of the probabilistic projections is the method of GMSL rise as in AR5 of the IPCC (Church et al., 2013) and extended by de Vries et al. (2014) and Le Bars et al. (2017). Here, only the modifications are presented with full details in the Supplement. New IPCC projections are now available from the Special Report on the Ocean and Cryosphere in a Changing Climate (SROCC) report (Oppenheimer et al., 2019). These projections are similar to AR5 except for the RCP8.5 scenario for which they are now around 10 cm higher because of a re-evaluation of the AIS contribution.

A rise in GMSL can be attributed to changes in mass loss from the Greenland ice sheet (GIS), AIS, glaciers and small ice caps (GIC) and land water (LW), and by thermal expansion and salinity changes of the ocean (ocean steric). Both ice sheets are further subdivided into a component that represents dynamic mass loss (dynamic processes at the ice-ocean boundary) and surface mass balance (mass changes due to accumulation and ablation). Regional SLR can differ from GMSL rise due to the self-gravitational and rotational effects of mass loss from the ice sheets, and changes in regional ocean dynamics and the inverse barometer (IB) effect (Slangen et al., 2014). Vertical ground motions are not included in the projections given contrasting estimates derived from different methodologies (see Supplement).

Three modifications are made relative to Church et al. (2013), namely (1) substitution of the AIS dynamics with two other estimates, (2) regional correlation between the ocean steric component and global mean surface temperature (GMST), and including additional model uncertainty in the projections.

(1) In AR5, the AIS dynamics contribution is included by means of a uniform, scenario-independent, distribution function with median of 8 cm. This was based on Little et al. (2013), who extrapolated observed growth rate of discharge in part of West Antarctica and further quantified the uncertainty about future discharge from other drainage basins on the AIS. For the second case, results from Levermann et al. (2014) are used. Linear response theory is used to construct a probabilistic framework combining the results of five ice sheet numerical models to project ice discharge for varying basal melt scenarios (melt underneath the ice shelves due to an influx of warm ocean water). The use of linear response theory implies that self-amplifying effects such as MICI and MISI are assumed not to be dominant. The result for both RCPs is a skewed distribution function with the median close to the median value of Church et al. (2013), but with increased probability of larger mass loss. The third case includes the numerical model results of DeConto and Pollard (2016). Their projections of AIS contribution to end-century GMSL are hitherto the highest reported values from a numerical model. The numerical model has, apart from MISI feedback, the first parametrisation of hydrofracturing due to surface melting and ice-cliff structural failure, leading to the MICI feedback (Pollard et al., 2015). As in Le Bars et al. (2017), we use the most extreme case from DP16, which assumes a SLR of 10 to 20 m during the Pliocene and applies a bias correction to the temperature of the ocean forcing in the Amundsen Sea and Bellingshausen Sea. The representation of the DP16 projections in (Le Bars et al., 2017) is simplified: the uncertainty is represented as a normal distribution instead of positively skewed (Kopp et al., 2017;

Edwards et al., 2019) and the temperature dependence for a given date is obtained from a linear interpolation between the RCP4.5 and RCP8.5 scenarios from DP16.

(2) The ocean steric component, ocean dynamics, IB and GMST are taken from an ensemble of global climate models; the Coupled Model Intercomparison Project Phase 5 (CMIP5). In AR5, the steric contribution to GMSL rise is assumed to be perfectly correlated with GMST ($\rho = 1.0$). However, for Sint Maarten, a local correlation coefficient of 0.4 is found from the CMIP5 models. The low local correlation can be well explained by the fact that steric effects are not only forced by GMST, but also depend on ocean dynamical processes that are model dependent (Le Bars, 2018). To account for the fact that the climate model range does not accurately represent the entire range of likely futures (Annan and Hargreaves, 2010), an additional model uncertainty is introduced by rescaling the model based 5-95th percentile range to the 17-83rd percentiles. This is implemented by multiplying the standard deviation of the normal distributions representing temperature and ocean thermal expansion by a factor 1.64, as done previously by Kopp et al. (2014) and Le Bars et al. (2017).

To construct regional SLR projections, the global projections of mass change are scaled to the local scale using fingerprint values of Slangen et al. (2012, 2014). In this region, the fingerprint for the AIS has a value 15 to 30% above the global average, whereas GIS, GIC and LW are close to the global average ($\sim$90-100%). Vertical land movement is excluded from the analysis given diverging local trends observed using different methods (see Supplement). This now results in regional SLR projections from 2006 to 2100 for the three cases of AIS dynamics and two representative concentration pathways (RCP); RCP4.5 and RCP8.5. Henceforth, we will abbreviate the different cases as IPCC, LEV14 and DP16.

2.3 Synthetic storm sampling

SSS allow sampling many plausible multi-variate storm time series (Callaghan et al., 2008; Li et al., 2014a; Wahl et al., 2016; Davies et al., 2017), which can be coupled to plausible SLR trajectories. The use of SSS intrinsically assumes that the observations represent only one realization of potentially observed storm parameters instead of the full envelop of realizations. To derive the SSS, we first create time series of storm parameters and extract storms from this. These storms are used to fit a stochastic model, from which random storm parameters can be sampled. Regional SLR trajectories can then be added to the storm surges to explore possible futures.

We extract data from satellite-based products that have a global coverage, which makes the approach generic and easily applicable in data-scarce environments.

2.3.1 Data retrieval

Storm parameters are here defined as a combination of wave and wind climate data (significant wave height H_s, peak wave period T_p, wave direction θ; wind speed u_{10}) and (storm) surge S. Time series of storm parameters are derived for a 25 year period (1993-2017) with 6h temporal resolution. H_s, T, θ and u_{10} are taken from the ERA-Interim reanalysis product (Dee et al., 2011). Data is extracted from an offshore loca-

tion [18.125°N, 62.875°W] (OB) and [18.0°N, 62.875°W] (DB), where water depth is considered deep enough to assume linear (Airy) wave theory. A time series of S is constructed by adding up the astronomical tide η_a (FES2014, Carrere et al., 2015), atmospheric wind and pressure set-up η_{sur} (Mog2D-G, Carrère and Lyard, 2003), extra wind set-up η_{wis} and wave set-up η_{was} (Dean and Dalrymple, 2001).The resolution of the reanalysis products is too coarse to resolve hurricanes in the region, thereby under estimating the erosion during hurricane events. η_{was} requires information on breaking wave height H_b and depth h_b. To translate offshore wave conditions to breaking wave height, the predictive formula of Larson et al. (2010) is applied. This predictive formula essentially governs the wave energy flux conservation combined with Snell's law.

Storm events are extracted from the 25 year time series. Here, we define a storm as an offshore wave height threshold that, if surpassed, will result in morphological change at the beach. Wave height is used as an indicator given that wave impact results in the mobilisation of sediments at the beach with the resulting undertow and rip currents moving the sediment offshore (van Rijn, 2009). Moreover, η_{was} dominates S, with contributions never less than 75-80%. Setting the threshold is however difficult, since we lack storm erosion data. To bridge this gap, satellite derived shoreline (SDS) positions from mid 2012 to early 2017 are obtained from Luijendijk et al. (2018). SDS are derived from satellite images that detect the shoreline using a shoreline detection algorithm. For the Sint Maarten beaches, the recurrence interval of satellite measurements is between 1 and 16 days over this period. From this, periods of shoreline erosion and accretion can be identified (Figure 1b), which show a clear seasonal cycle. We adopt an iterative approach of setting the wave height threshold, identifying storms and comparing the times when storms are identified with the instances when the shoreline is eroding. For both beaches, a threshold is set to 1.9 m that explains most instances when the shoreline is eroding (or already eroded). For Orient Bay, this is indicated by the grey lines in Figure 1 together with the corresponding values of H_s and S.

2.3.2 Implementation synthetic storm time series

From the storms identified in the time series, we extract storm parameters: peak H_s, peak S, the concordant T_P and θ of the peak H_s, monthly storm frequency (F_s), and the duration of the storm D above the threshold. To extract independent events, a 24h time interval time is set that has to be exceeded before a new storm is counted, following Li et al. (2014b). Moreover, storms are split into summer storms (April-September) and winter storms (November-March), to account for the seasonality that exists. Mathematical details and further details of the method are included in the Supplement.

To model interdependencies between storm parameters, we use copulas. A copula can be defined as a joint distribution function on unit scale [0 1] (Sklar, 1959), which makes them very flexible, as they are independent of the underlying marginal distribution function of the variables (de Waal and van Gelder, 2005). A copula is fitted to the interdependencies $H_s - S$, $H_s - D$ and $H_s - T_p$ for both seasons. We test both elliptical (Gaussian and t) and Archimedean copulas (Frank, Gumbel, Clayton),

and perform a goodness-of-fit test based on *Cramèr-von Mises* $\mathscr{M}$ statistic (Genest et al., 2009). The *t*-copula is taken, which performs well and has the advantage that it can be extended to multiple dimensions easily (characteristic of elliptical copulas). This copula in combination with the marginal distribution function (MDF) per variable is used to sample a four-dimensional set of the storm parameters (H_s, T_p, S, D) per synthetic storm event. θ is sampled independently from its empirical cumulative distribution function (ECDF), while only considering wave angles within the range of incident angles. For F_s, a Poisson distribution is fitted to the monthly rate of storm occurrences (making yearly storm occurrence also Poisson distributed). From this, a random sample can be drawn for every month, with storms assigned a time stamp within a month (maintaining a 24h inter-arrival time between storms).

To constrain the samples within a physically realistic extent, a few boundaries are set (dashed line Figure 2). Observations show a maximum steepness of $s = 0.06$ between wave length (thus wave period) and a maximum duration of D = 350h. Additionally, following Wahl et al. (2016), the maximum wave period is fixed at 25 s, to avoid sampling waves that are being classified as infragravity waves (Munk, 1949). A trend analysis of (seasonal) storm parameters, similar to Wahl and Plant (2015), is performed. Results suggest that the seasonal cycle is slightly amplified (positive in winter, negative in summer) over the period 1993-2017. In contrast, climate models predict a small decline in wave and surge conditions for the future (Hemer et al., 2013; Vousdoukas et al., 2018). It is therefore chosen to assume stationary storm conditions for the SSS.

Now, many long time series of future storm events can be sampled. This is exemplified in Figure 2 where 10,000 samples are generated and compared to the observations in blue (winter) and red (summer) together with the MDF, clearly showing a seasonal difference in dependency structure (hence different copulas). The rank correlations (ρ_r) of the observations (black) resemble those of the seasonal copulas (red/blue).

SLR projections are constructed for the period 2006-2100, and so SSS are also made for the same time period (95 years). SLR will gradually increase over the years and adds up to the S that is sampled by the copula ($S_{slr,yr} = S_{yr} + SLR_{yr}$). A SLR trajectory is constructed by random sampling from the distribution function of SLR. For instance, a 50th percentile trajectory consists of the 50th percentile values per year. This SLR trajectory can then be added to the S values sampled for the corresponding years.

2.4 Storm erosion and shoreline position

Coastal morphological response to storm events and SLR is expressed by two parameters; the short-term retreat distance due to individual storms (*RD*) and the long-term coastal recession (*CR*).

To model *RD*, an analytical formula derived by Kriebel and Dean (1993) (henceforth KD93) is used that is fed by the storm parameters of the SSS. The KD93 formulation has no calibration parameter and is therefore applied using the recommended settings (see Supplement). After a storm has eroded the beach, wave driven transport

and aeolian processes will move sediment back to the beach and (partly) recover it before a new storm hits. With SLR, however, the magnitude of storm erosion will gradually increase and the beach does not have enough time to recover from extreme events (because extreme events are occurring more frequently). This drives a net sediment loss over the years, hence long-term *CR* of the coast. To forecast the shoreline position, the shoreline movements in between storm events also need to be quantified. We follow an approach similar to Ranasinghe et al. (2012) using a linear recovery rate, but deviate by introducing a simple state dependency (see Supplement). The state dependency is introduced since it is known that the rate of shoreline change is, apart from wave energy, determined by its antecedent position (Yates et al., 2009). We search for a representative recovery rate of the system that, on average, stabilizes the coast under a 500 yr simulation time in absence of SLR (storm forcing only). For Orient Bay, a representative recovery rate of 0.10 m day^{-1} is found, whereas for Dawn Beach this recovery rate is 0.165 m day^{-1}. If SLR is now added in the simulations, the beach will gradually erode over time and the *CR* for a given year can be determined.

To validate the variability of the shoreline, the standard deviation of the detrended ECDF of SDS data and the 500 yr model run (without SLR) are compared. The standard deviation is a measure of the 'beach mobility' (Stive et al., 2002) and shows good agreement (Supplement).

2.5 Sampling and analysis

The above described methodology can be repeated multiple times. This is done as follows; (1) sample a SSS together with a SLR pathway for 2006-2100, (2) calculate retreat distances due to storms and SLR, (3) forecast the shoreline behaviour using the recovery rate, (4) analyse the erosion hazard over the 95 year period, (5) repeat 10,000 times to obtain probabilistic estimates for all SLR cases.

For *RD*, a generalized Pareto distribution is fitted to the data and the return periods are calculated over the 2006-2100 period. The average shoreline position in 2100 is used to obtain *CR* estimates for 2100 compared to 2006.

3 Results

3.1 Regional sea-level rise

The results for IPCC, LEV14 and DP16 cases for 2100 compared to the 1986-2005 average are shown in Figure 3b&d. The median (95th percentile) value of DP16 is respectively 200 (266) cm for RCP8.5 and 108 (184) cm for RCP4.5. The skewed distribution function of the LEV14 case has a median value (95th percentile value) of 81 (134) cm for RCP8.5 and 57 (95) cm for RCP4.5. In contrast, the IPCC estimates reach 74 (111) cm and 54 (80) cm for the same percentiles and climate scenarios. Until 2060, results do not notably differ. Relative to GMSL rise, median SLR along the Sint Maarten coast will be 1.01-1.14 times larger.

3.2 Retreat distance and recession

Future return period of storm erosion over the years 2006-2100, including the 90% uncertainty range, are provided in Figure 4a-d. For comparison, the black line in Figures 4a-d is the baseline case without SLR. We define return periods as the average rate of occurrence of an event integrated over a given time span, here from 2006 till 2100. For instance, the 1/50 year will thus happen approximately twice over this period. For Orient Bay the return period of a 1/100 year retreat event is 1.67 (2.4) times higher for DP16 and around 1.4 (1.5) times higher for LEV14 and IPCC compared to the baseline under RCP4.5 (RCP8.5).

Supplementary Figure 3a-d shows the correlation between the SLR-value for a given year x and the 1/100 year retreat distance over the years (thus from 2006 to year x). The SLR value sampled determines the trajectory taken. In case of a low correlation, the SLR trajectory sampled was apparently not a driving force for the 1/100 year erosion event (storm randomness dominates). Until 2060-2070, the correlation is still below 0.5 implying a moderate dependency. Thus, the increased frequency of more extreme *S* will not alter the extreme value statistics much. For Orient Bay, the correlations in 2100 are close to 0.8-0.9 meaning that SLR is steering the extreme *RD* over the storm randomness, whereas for Dawn Beach this influence is less pronounced. The difference between the two beaches can also be explained physically. Dawn Beach has a steeper beach slope and foreshore slope. According to Kriebel and Dean (1993), this yields a more reactive beach in terms of morphological response. This makes it less sensitive to an increase in *S* and more sensitive to the other storm parameters influencing *RD*.

Finally, *CR* for 2100 is summarized in Figure 5. First of all, Dawn Beach (Figure 5c&d) will experience larger *CR*, in line with the larger retreat distances, influenced by the morphological character of the Beach. Median *CR* values (black circle) range from 6-22 m for Dawn beach and 5-16 m for Orient Bay. However, the 1% exceedance probability (thin line upper panel) ranges from 13-45 m for Dawn Beach and 9-38 m for Orient Bay (Figure 5a&b). The lower value of the range corresponds to the IPCC case, whereas the upper range corresponds to the DP16 case, a 3.2-4.2 factor difference.

4 Discussion

4.1 Implications for design of coastal defences

The sensitivity of future erosion estimates to the ambiguity of AIS dynamics have implications for the design of coastal defences.

For the retreat distance due to storms, we consider the estimates of the IPCC sea level projections for every return period and search for the relative return period for the other two cases (e.g. a 1/100 yr event has a value of 30 m for IPCC. 30m corresponds to a 1/x yr return period for LEV14). The result of this is displayed in Figure 4i-l. The dashed black line indicates perfect alignment between the cases with larger deviation from this line indicating larger difference. For instance, consider a

coastal manager designing a setback line based on the 1/100 yr erosion event using the median value of the IPCC projections. This event may, however, only be a 1/70 (1/60) event for LEV14 (solid blue line) and a 1/12 (1/2) event for DP16 (solid red line) for RCP4.5 (RCP8.5) at Orient Bay. Therefore, this threshold will occur 1.4-1.67 times as frequently for LEV14 and 8.3-50 times as frequently for DP16 over the same time span, with potential large economic consequences (e.g. tourism, damage coastal infrastructure). For Dawn Beach, this effect is slightly less with relative return periods of 1/90 (1/80) for LEV14 and 1/35 (1/7) for DP16 given scenario RCP4.5 (RCP8.5). For larger return periods and for higher percentiles (dashed blue and red line Figure 4i-l), the relative difference increases. Therefore, paradoxically, risk-averse coastal managers, implementing additional safety into their design standards, may make a larger underestimation relative to their risk preference.

A similar analysis can be done for coastal recession by comparing the 2100 estimates relative to 2006 expressed in terms of exceedance probability (Figure 5e-h). Again, larger deviations from the linear line (dashed black line) indicate larger differences (but now above this line). Here also larger relative differences are found for the lower exceedance probabilities. Now consider a coastal manager that designs a sand nourishments to counterbalance the projected future erosion equal to a 1% exceedance probability for the median IPCC case. In contrast, this same design value has a 3-4.5% exceedance probability for LEV14 and a 37-72% exceedance probability under DP16. This may be unacceptable in terms of risk faced by the coastal community or may alter the cost-efficiency and lifespan of the nourishment as additional sand is necessary. We compare the recession values of the IPCC case in 2100 with the two other cases and search for the year where this value will be reached. This is done for a few exceedance probabilities and shown in Supplementary Figure 3. For DP16, the same exceedance probabilities for the IPCC case will be reached 20-25 years earlier, almost independent on the exceedance probability adopted. For LEV14, on the contrary, there is a dependency on the exceedance probability adopted, and the acceleration in terms of years is between 2 and 15 years.

Therefore, taking the uncertainty of AIS dynamics into account is critical for the design of coastal protection measures. Other approaches than comparing three cases exist to do this, such as extra-probability theory (Le Cozannet et al., 2017) or expert elicitation (Bamber and Aspinall, 2013; Oppenheimer et al., 2016). It also becomes evident from the comparison between the beaches and the correlation analysis that the morphological characteristics, and uncertainties, may be as important for the future erosion estimates as the SLR projections and uncertainties, which agrees well with previous research Le Cozannet et al. (2019). This makes it important to consider morphological heterogeneity in future work that look at regional and global scale analysis of erosion. New global datasets on morphological parameters can steer this development (Athanasiou et al., 2019).

4.2 Application and extension to other beaches

Although our results are presented for two beaches, the method can be easily extrapolated to other sandy beaches globally. However, some local characteristics may in-

fluence the results and modelling decisions made. First, we only consider cross-shore morphological change which can be substantiated by the fact the satellite-derived shoreline data does not show a clear trend in long-term shoreline change. Our approach could be extended by considering all sources and sinks of the sediment budget (Dean and Houston, 2016), which might be a dominant driver at other beaches (Luijendijk et al., 2018). Second, we do not account for interannual and multidecadal variability in storm parameters, which may dampen or amplify erosion risk at some places (Wahl and Plant, 2015; Davies et al., 2017). Variability can often be linked to large scale atmospheric dynamics. In our area, for instance, we find a negative correlation between the monthly Niño3.4-index and monthly H_s ($\rho \sim$ -0.35). Third, improvement can be made for the inclusion of erosion induced by hurricanes, since hurricanes are not well captured using the re-analysis data and can govern the design standards of mitigation measures. Recent advances in forcing large-scale hydrodynamic models with observed or synthetic hurricanes (Marsooli et al., 2019; Bloemendaal et al., 2020) can help refine the occurrence of extreme surges and hence erosion. Fourth for the coastal impact model, the Kriebel and Dean (1993) formulation is considered suitable for first-order estimates of beach erosion and it is thought to be most suitable for the beaches under consideration. In contrast, for beaches with more dune-like features, other analytical formulas may be more suitable (e.g. Larson et al., 2004). When higher accuracy is required, a semi-empirical model (Callaghan et al., 2013) can be considered. At last, we assume a linear recovery rate of the beach, which are close to the linear recovery rates mentioned in literature (summarized in Phillips et al., 2017) and identified in the SDS. Dune/beach recovery, however, is coupled to marine and aeolian processes (Cohn et al., 2018), which differ per beach, making the recovery rate variable over space and time. Therefore, local erosion measurements may improve the validation of modelling choices and variables.

5 Conclusions

The aim of this study was to evaluate the influence of three formulations of AIS dynamics into regional SLR projections on future coastal erosion that inform coastal defences. A probabilistic approach was adopted that combines regional SLR projections with synthetic storm time series and analytical storm erosion and shoreline prediction model.

We find that SLR uncertainties has an important contribution to 21st century estimates of storm erosion events, and dominate the erosion response after 2070. Estimates of future erosion hazard tends to be prone to the assumptions made on how to include the AIS dynamics into SLR projections. We estimate that return periods of future design storm erosion may differ up to a factor 50 under various AIS scenarios. In terms of longer term recession, estimates of exceedance probability (by 2100) differ by up to a factor 72 and a given recession value may therefore be reached 2-25 years ahead of 2100. In general, larger return periods and low-exceedance probabilities are relatively more sensitive to the various AIS dynamics scenarios. Moreover, we find that heterogeneity in morphological factors, and sensitivity to storm parameters (due

to exposure), may be equally important as SLR uncertainties, and hence should be a focus point to better understand the sensitivity of global coastlines to SLR.

From our analysis, we conclude that precluding AIS uncertainty from SLR projections that feed into coastal impact assessments may lead to ill-informed adaptation decisions, alter the cost-efficiency of coastal defences, and lead to potentially intolerable risk.

Acknowledgements The authors would like to thank Arjen Luijendijk for providing the satellite derived shoreline positions of the Sint Maarten beaches. We further would like to acknowledge Ali Dastgheib for fruitful discussions during the research. RR is supported by the AXA Research fund and the Deltares Strategic Research Programme Coastal and Offshore Engineering.

References

Anderson TR, Fletcher CH, Barbee MM, Frazer LN, Romine BM (2015) Doubling of coastal erosion under rising sea level by mid-century in Hawaii. Nat Hazards 78(1):75–103, DOI 10.1007/s11069-015-1698-6

Annan J, Hargreaves J (2010) Reliability of the CMIP3 ensemble. Geophys Res Lett 37(L02703):1–5

Athanasiou P, Van Dongeren A, Giardino A, Vousdoukas M, Gaytan-Aguilar S, Ranasinghe R (2019) Global distribution of nearshore slopes with implications for coastal retreat. Earth System Science Data 11(4):1515–1529, DOI 10.5194/essd-11-1515-2019

Bamber J, Aspinall W (2013) An expert judgement assessment of future sea level rise from the ice sheets. Nat Clim Change 3:424–428

Bloemendaal N, Haigh ID, de Moel H, Muis S, Haarsma RJ, Aerts JCJH (2020) Generation of a global synthetic tropical cyclone hazard dataset using STORM. Sci Data 7(1):40, DOI 10.1038/s41597-020-0381-2, URL http://dx.doi.org/10.1038/s41597-020-0381-2 http://www.nature.com/articles/s41597-020-0381-2

Boon J, Green MO (1988) Caribbean beach-face slopes and beach equilibrium profiles. Coast Eng 120:1618–1630

Bruun P (1954) Coast erosion and the development of beach profiles, beach erosion board technical memorandum. Tech. rep., U.S. Army Engineer Waterways Experiment Station. Vicksburg, MS

Buchanan M, Oppenheimer M, Kopp R (2017) Amplification of flood frequencies with local sea level rise and emerging flood regimes. Environ Res Lett 12(064009):1–7

Callaghan D, Nielson P, Short A, Ranasinghe R (2008) Statistical simulation of wave climate and extreme beach erosion. Coast Eng 55:375–390

Callaghan DP, Roshanka R, Andrew S (2009) Quantifying the storm erosion hazard for coastal planning. Coast Eng 56(1):90–93, DOI 10.1016/j.coastaleng.2008.10.003

Callaghan DP, Ranasinghe R, Roelvink D (2013) Probabilistic estimation of storm erosion using analytical, semi-empirical, and process based storm erosion models. Coast Eng 82:64–75, DOI 10.1016/j.coastaleng.2013.08.007

Carley J, Cox R (2003) A methodology for utilising time- dependent beach erosion models for design events. In: Proceedings of the 16th Australasian Coastal and Ocean Engineering Conference, Auckland, New Zealand

Carrère L, Lyard F (2003) Modeling the barotropic response of the global ocean to atmospheric wind and pressure forcing - Comparisons with observations. Geophys Res Lett 30(6):1997–2000, DOI 10.1029/2002GL016473

Carrere L, Lyard F, Cancet M, Guillot A (2015) FES 2014, a new tidal model on the global ocean with enhanced accuracy in shallow seas and in the Arctic region. EGU General Assembly Conference Abstracts 17:5481

Church J, Clark P, Cazenave A, Gregory J, Jevrejeva S, Levermann A, Merrifield M, Milne G, Nerem R, Nunn P, Payne A, Pfeffer W, Stammer D, Unnikrishan A (2013) Sea level change. in: Climate change 2013: The physical science basis. contribution

of working group i to the fifth assessment report of the intergovernmental panel on climate change. Tech. rep., Cambridge University Press, Cambridge, United Kingdom and New York, NY, USA.

Cohn N, Ruggiero P, de Vries S, Kaminsky GM (2018) New Insights on Coastal Foredune Growth: The Relative Contributions of Marine and Aeolian Processes. Geophys Res Lett 45:4965–4973, DOI 10.1029/2018GL077836

Cooper J, Pilkey O (2004) Sea-level rise and shoreline retreat: time to abandon the bruun rule. Global Planet Change 43:157–171

Corbella S, Stretch D (2012) Predicting coastal erosion trends using non-stationary statistics and process-based models. Coast Eng 70:40–49

Cowell PJ, Thom BG, Jones RA, Everts CH, Simanovic D (2006) Management of Uncertainty in Predicting Climate-Change Impacts on Beaches. J Coast Res 221:232–245, DOI 10.2112/05A-0018.1

Dastgheib A, Jongejan R, Wickramanayake M, Ranasinghe R (2018) Regional scale risk-informed land-use planning using probabilistic coastline recession modelling and economical optimisation: East coast of Sri Lanka. J Mar Sci Eng in review

Davies G, Callaghan DP, Gravios U, Jiang W, Hanslow D, Nichol S, Baldock T (2017) Improved treatment of non-stationary conditions and uncertainties in probabilistic models of storm wave climate. Coast Eng 127(June):1–19, DOI 10.1016/j.coastaleng.2017.06.005

de Waal D, van Gelder P (2005) Modelling of extreme wave heights and periods through copulas. Extremes 8:345–356

Dean R, Dalrymple R (2001) Coastal processes with engineering applications. Cambridge University Press, Cambridge

Dean R, Houston J (2016) Determining shoreline response to sea level rise. Coast Eng 114:1–8

DeConto RM, Pollard D (2016) Contribution of Antarctica to past and future sea-level rise. Nature 531(7596):591–597, DOI 10.1038/nature17145

Dee D, Uppala S, Simmonds A, Berrisford P, Poli P, Kobayashi S, Andrae U, et al (2011) The era-interim reanalysis: configuration and performance of the data assimilation system. Q J Roy Meteorol Soc 137:553–597

Edwards TL, Brandon MA, Durand G, Edwards NR, Golledge NR, Holden PB, Nias IJ, Payne AJ, Ritz C, Wernecke A (2019) Revisiting Antarctic ice loss due to marine ice-cliff instability. Nature 566(7742):58–64, DOI 10.1038/s41586-019-0901-4, URL http://dx.doi.org/10.1038/s41586-019-0901-4

FitzGerald D, Fenster M, andIV Buynevich BA (2008) Coastal impacts due to sea-level rise. Annu Rev Earth Planet Sci 36:601–647

Genest C, Rémillard B, Beaudoin D (2009) Goodness-of-fit tests for copulas: A review and a power study. Insur Math Econ 44(2):199–213, DOI 10.1016/j.insmatheco.2007.10.005

Hallegatte S, Green C, Nicholls RJ, Corfee-Morlot J (2013) Future flood losses in major coastal cities. Nat Clim Change 3(9):802–806, DOI 10.1038/nclimate1979

Hemer M, Fan Y, Mori N, Semedo A, Wang X (2013) Projected changes in wave climate from a multi-model ensemble. Nat Clim Change 3:471–476

Hinkel J, Nicholls R, Tol R, Wang Z, Hamilton J, Boot G, Vafeidis A, McFadden L, Ganopolski A, Klein R (2013) A global analysis of erosion of sandy beaches and

sea level rise: an application of diva. Global Planet Change 111:150–158
Hinkel J, Jaeger C, Nicholls R, Lowe J, Renn O, Reijun S (2015) Sea-level rise scenarios and coastal risk management. Nat Clim Change 5:188–191
Jongejan R, Ranasinghe R, Wainwright D, Callaghan D, Reyns J (2016) Drawing the line on coastline recession risk. Ocean and Coastal Management 122:87–94
Joughin I, Smith BE, Medley B (2014) Marine Ice Sheet Collapse Potentially Under Way for the Thwaites Glacier Basin, West Antarctica. Science 344(6185):735–738, DOI 10.1126/science.1249055
Jury M (2018) Characteristics and meteorology of atlantic swells reaching the caribbean. J Coast Res 34(2):400–412
Kjerfve B (1981) Tides of the caribbean. J Geophys Res 86(C5):4243–4247
Kopp R, Horton R, Little C, Mitrovica J, Oppenheimer M, Rasmussen D, Strauss B, Tebaldi C (2014) Probabilistic 21st and 22nd century sea-level projections at a global network of tide-gauge sites. Earth's Future 2:383–406
Kopp R, DeConto R, Bader D, Hay C, Horton R, Kulp S, Oppenheimer M, Pollard D (2017) Evolving understanding of antarctic ice-sheet physics and ambiguity in probabilistic sea-level projections. Earth's Future 5:1–17
Kriebel D, Dean R (1993) Convolution method for time-dependent beach-profile response. J Waterw Port Coast 119(2):204–226
Larson M, Erikson L, Hanson H (2004) An analytical model to predict dune erosion due to wave impact. Coast Eng 51:675–696
Larson M, Hoan L, Hanson H (2010) Direct formula to compute wave height and angle at incipient breaking. J Waterw Port Coast 136(2):119–122
Le Bars D (2018) Uncertainty in Sea Level Rise Projections Due to the Dependence Between Contributors. Earth's Future 6:1–17, DOI 10.1029/2018EF000849
Le Bars D, Drijfhout S, de Vries H (2017) A high-end sea level rise probabilitic projection including rapid antarctic ice sheet mass loss. Environ Res Lett 12(044013):1–10
Le Cozannet G, Manceau J, Rohmer J (2017) Bounding probabilistic sea-level projections within the framework of the possibility theory. Environ Res Lett 12(014012):1–11
Le Cozannet G, Bulteau T, Castelle B, Ranasinghe R, Wöppelmann G, Rohmer J, Bernon N, Idier D, Louisor J, Salas-y Mélia D (2019) Quantifying uncertainties of sandy shoreline change projections as sea level rises. Scientific Reports 9(1):1–11, DOI 10.1038/s41598-018-37017-4
Levermann A, Winkelmann R, Nowicki S, Fastook J, Frieler K, Greve R, Helmer H, Martin M, Meinshausen M, Mengel M, Payne A, Pollard D, Sato T, Timmermann R, Wang W, Bindschadler R (2014) Projecting antarctic ice discharge using response functions from searise ice-sheet models. Earth Syst Dynam 5:271–293
Li F, van Gelder P, Ranasinghe R, Callaghan D, Jongejan R (2014a) Probabilistic modelling of extreme storms along the Dutch coast. Coast Eng 86:1–13, DOI 10.1016/j.coastaleng.2013.12.009
Li F, van Gelder P, Vrijling J, Callaghan D, Jongejan R, Ranasinghe R (2014b) Probabilistic estimation of coastal dune erosion and recession by statistical simulation of storm events. Appl Ocean Res 47:53–62, DOI 10.1016/j.apor.2014.01.002

Little C, Urban N, Oppenheimer M (2013) Probabilistic framework for assessing the ice sheet contribution to sea level change. PNAS 110(9):3264–3269

Luijendijk A, Hagenaars G, Ranasinghe R, Baart F, Donchyts G, Aarninkhof S (2018) The state of the world's beaches. Sci Rep 8(6641):1–11

Marsooli R, Lin N, Emanuel K, Feng K (2019) Climate change exacerbates hurricane flood hazards along US Atlantic and Gulf Coasts in spatially varying patterns. Nat Commun 10(1):1–9, DOI 10.1038/s41467-019-11755-z

McGranahan G, Balk D, Anderson B (2007) The rising tide: assessing the risks of climate change and human settlements in low elevation coastal zones. Environ Urban 19(1):17–37

McInnes KL, White CJ, Haigh ID, Hemer MA, Hoeke RK, Holbrook NJ, Kiem AS, Oliver EC, Ranasinghe R, Walsh KJ, Westra S, Cox R (2016) Natural hazards in Australia: sea level and coastal extremes. Climatic Change 139(1):69–83, DOI 10.1007/s10584-016-1647-8

Munk WH (1949) Surf beats. Transaction American Geophysical Union 30(6)

Oppenheimer M, Alley R (2016) How high will the seas rise? Science 354(6318):1375–1376

Oppenheimer M, Little CM, Cooke RM (2016) Expert judgement and uncertainty quantification for climate change. Nat Clim Change 6(5):445–451, DOI 10.1038/nclimate2959

Oppenheimer M, Glavovic B, JR H, van de Wal R, Magnan A, Abd-Elgawad A, Cai R, Cifuentes-Jara M, DeConto R, Ghosh T, Hay J, Isla F, Marzeion B, Meyssignac B, Sebesvari Z (2019) IPCC Special Report on the Ocean and Cryosphere in a Changing Climate, in press, chap Sea Level Rise and Implications for Low-Lying Islands, Coasts and Communities

Phillips MS, Harley MD, Turner IL, Splinter KD, Cox RJ (2017) Shoreline recovery on wave-dominated sandy coastlines: the role of sandbar morphodynamics and nearshore wave parameters. Mar Geol 385:146–159, DOI 10.1016/j.margeo.2017.01.005

Pollard D, DeConto RM, Alley RB (2015) Potential Antarctic Ice Sheet retreat driven by hydrofracturing and ice cliff failure. Earth Planet Sci Lett 412:112–121, DOI 10.1016/j.epsl.2014.12.035

Ranasinghe R (2016) Assessing climate change impacts on open sandy coasts: A review. Earth Sci Rev 160:320–332, DOI 10.1016/j.earscirev.2016.07.011

Ranasinghe R, Stive MJF (2009) Rising seas and retreating coastlines. Climatic Change 97(3-4):465–468, DOI 10.1007/s10584-009-9593-3

Ranasinghe R, Callaghan D, Stive M (2012) Estimating coastal recession due to sea level rise: beyond the bruun rule. Climatic Change 110:561–574

Ritz C, Edwards T, Durand G, Payne A, Peyaud V, RCA H (2015) Potential sea-level rise from antarctic ice-sheet instability constrained by observations. Nature 528:115–129

Sklar A (1959) Fonctions de repartition a n dimensions et leurs marges. De, Publications and l'Institut de Statistique de Paris

Slangen A, Carson M, Katsman C, van der Wal R, Kohl A, Vermeersen L, DStammer (2014) Projecting twenty-first century regional sea-level changes. Climatic Change 124(1-2):317–332

Slangen ABA, Katsman CA, van de Wal RSW, Vermeersen LLA, Riva REM (2012) Towards regional projections of twenty-first century sea-level change based on IPCC SRES scenarios. Clim Dynam 38(5-6):1191–1209, DOI 10.1007/s00382-011-1057-6

Stive MJ, Aarninkhof SG, Hamm L, Hanson H, Larson M, Wijnberg KM, Nicholls RJ, Capobianco M (2002) Variability of shore and shoreline evolution. Coast Eng 47(2):211–235, DOI 10.1016/S0378-3839(02)00126-6

Stive MJF (2004) How important is global warming for coastal erosion? Climatic Change 64(1):27–39, DOI 10.1023/B:CLIM.0000024785.91858.1d

Tebaldi C, Strauss BH, Zervas CE (2012) Modelling sea level rise impacts on storm surges along US coasts. Environ Res Lett 7(1), DOI 10.1088/1748-9326/7/1/014032

Toimil A, Losada IJ, Camus P, Díaz-Simal P (2017) Managing coastal erosion under climate change at the regional scale. Coast Eng 128(July):106–122

van Rijn LC (2009) Prediction of dune erosion due to storms. Coast Eng 56(4):441–457, DOI 10.1016/j.coastaleng.2008.10.006

Vousdoukas MI, Mentaschi L, Voukouvalas E, Verlaan M, Jevrejeva S, Jackson LP, Feyen L (2018) Global probabilistic projections of extreme sea levels show intensification of coastal flood hazard. Nat Comm 9(1):2360, DOI 10.1038/s41467-018-04692-w

de Vries H, Katsman C, Drijfhout S (2014) Constructing scenarios of regional sea level change using global temperature pathways. Environ Res Lett 9(115007):1–8

Wahl T, Plant NG (2015) Changes in erosion and flooding risk due to long-term and cyclic oceanographic trends. Geophys Res Lett 42(8):2943–2950, DOI 10.1002/2015GL063876

Wahl T, Plant N, Long J (2016) Probabilistic assessment of erosion and flooding risk in the northern gulf of mexico. J Geophys Res C Oceans 121:3029–3042

Yates ML, Guza RT, O'Reilly WC (2009) Equilibrium shoreline response: Observations and modeling. J Geophys Res C Oceans 114(9):1–16, DOI 10.1029/2009JC005359

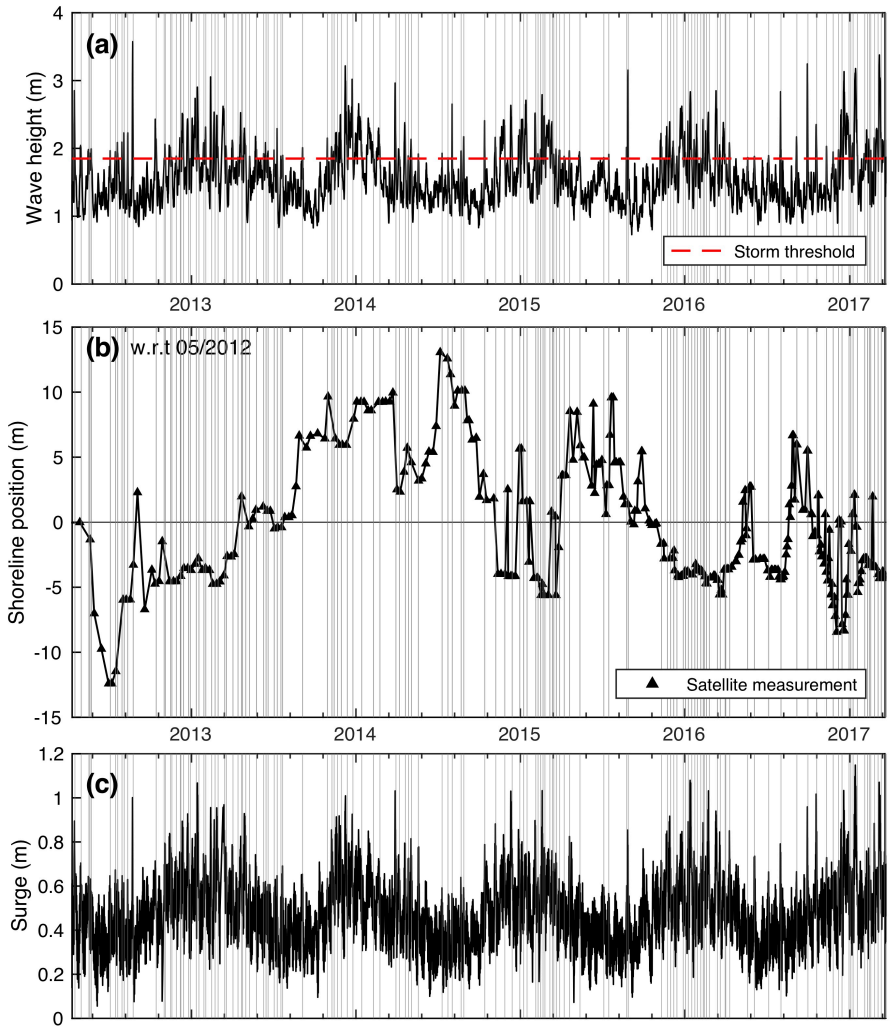

Fig. 1 (a) Time series of H_s together with the storm threshold of 1.9 m (red line). (b) Satellite derived shoreline (SDS) positions of Orient Bay with linear interpolation between SDS measurements (triangles). The shoreline position is relative to the position on March, 2012. (c) Time series of S. The grey line in (a-c) indicate the onset of the storm events as identified by the threshold.

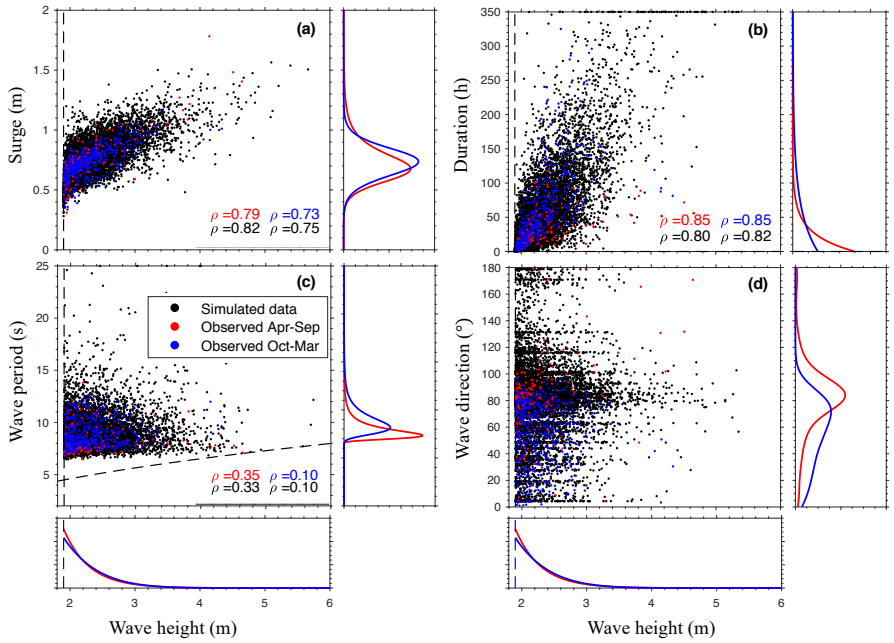

Fig. 2 (a) Scatterplot of observed variables H_s and S for both winter months (blue) and summer months (red). The black dots show a 10,000 random sample using the copulas. In the boxes, The univariate marginal distribution functions are shown in the boxed. Spearman rank correlation (ρ_r) of the seasonal observations (red and blue) are compared to those obtained from the sampled copula (black). (b) same as (a) but for H_s-D. (c) same as (a) but for H_s-T_p. Black dashed line indicate the steepness limit set ($s = 0.06$). (d) Same as (a) but for $H_s$and θ that is sampled independently from the empirical cumulative distribution function (no correlation compared).

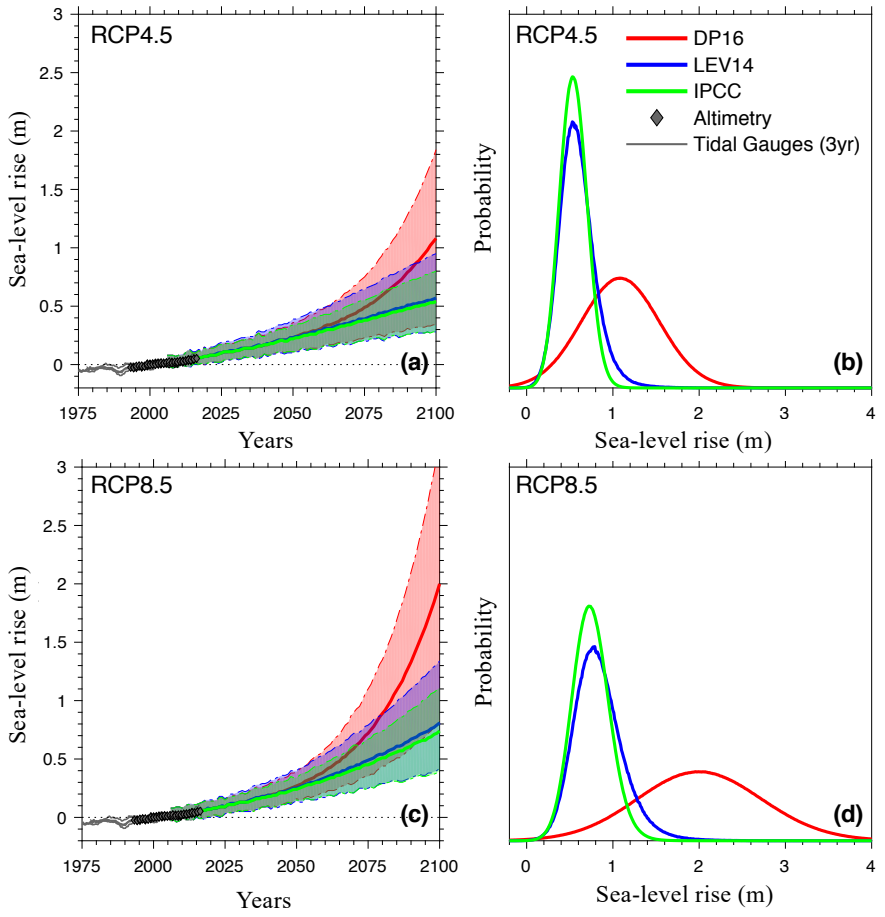

Fig. 3 (a) Regional SLR projections from 2006 to 2100 for RCP4.5. Grey line indicate 3 year running average of tidal gauge stations (PSMSL) and grey diamonds recent altimetry data (*aviso.altimetry.fr*) for the Caribbean. (b) PDFs of 2100 regional SLR compared to 1986-2005 under RCP4.5. (c-d) same as (a-b) but for RCP8.5.

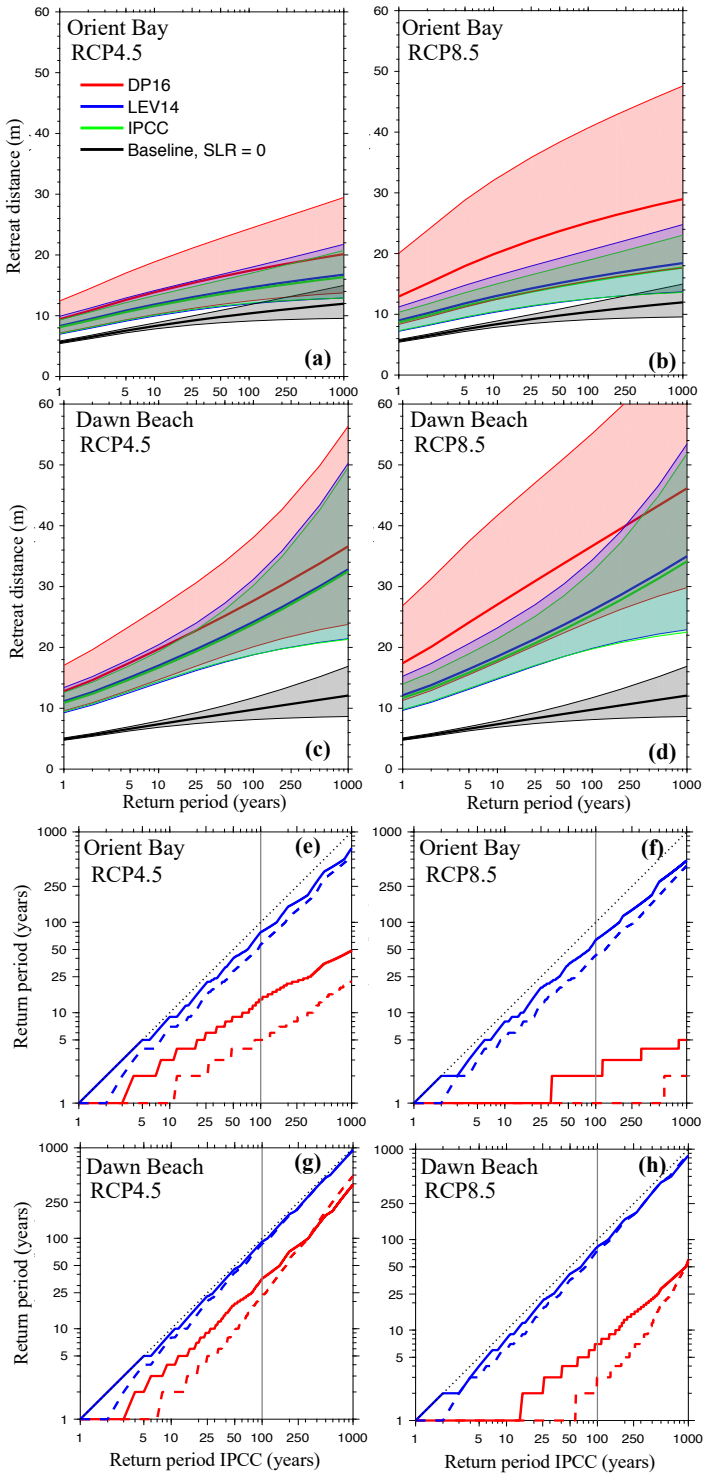

Fig. 4 (a) Return periods of retreat distance due to storm events over the period 2006-2100 for Orient Bay under RCP4.5. Median value (solid line) together with the 90% uncertainty (shaded area). (b) same as (a) but under RCP8.5. (c-d) same as (a-b) but for Orient Bay. (e) Comparison between return periods of retreat distance from storm events under the IPCC scenario and the DP16 (red) and LEV14 (blue) scenario. The dashed black line indicate perfect agreement (no difference). (f-h) same as (e) but for different RCP and different beach.

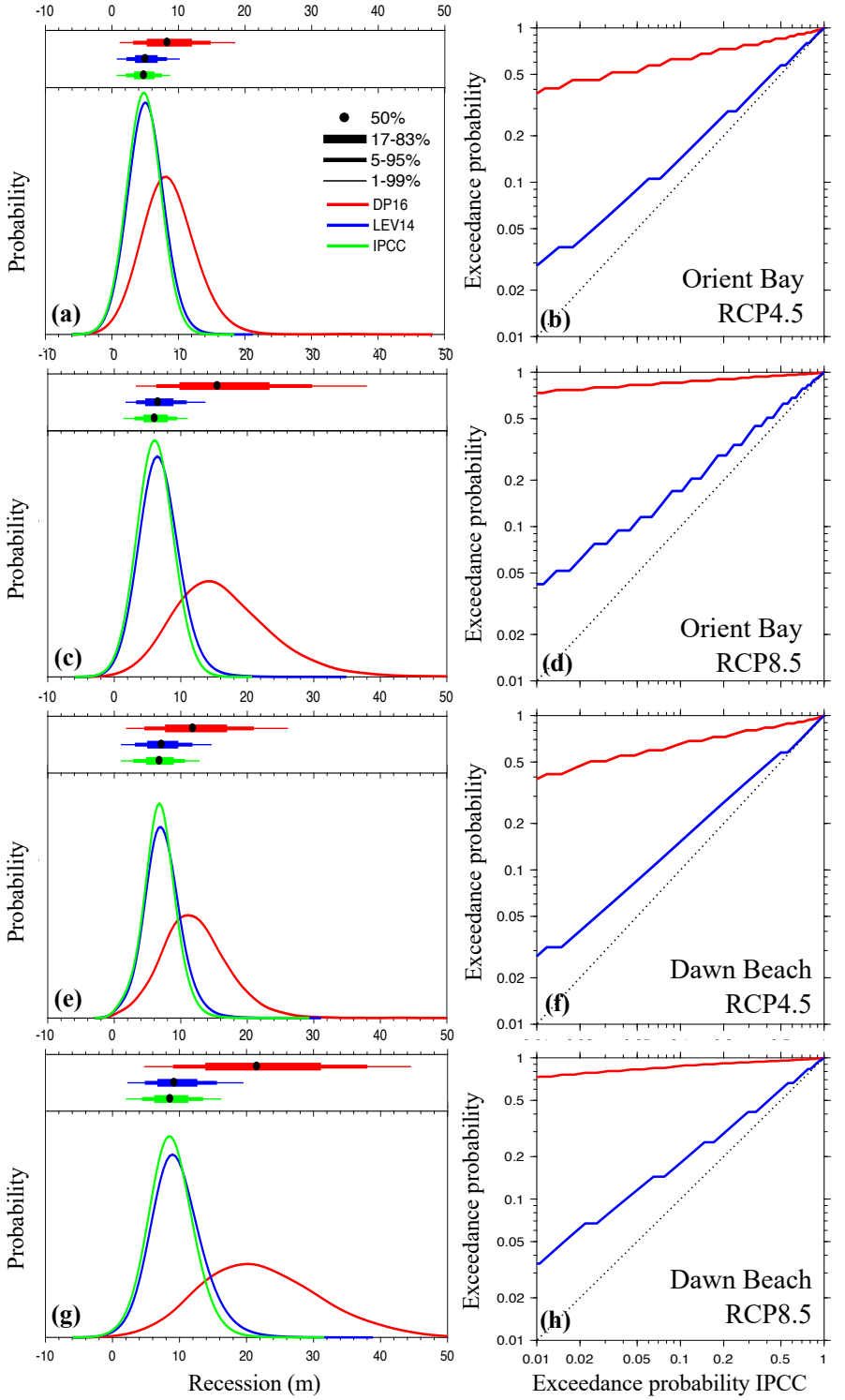

Fig. 5 (a) PDFs of 2100 recession values compared to 2006 for Orient Bay under RCP4.5. In the top panel, the median is shown together with the 66%, 90% and 98% uncertainty range. (b) same as (a) but for RCP4.5. (c-d) same as (a-b) but for Dawn Beach. (e) Comparison between exceedance probabilities of recession values in 2100 compared to 2006 under the IPCC scenario and the DP16 (red) and LEV14 (blue) scenario. (f-h) same as (e) but for RCP 8.5 (f) and for Dawn Beach (g-h).